QUADRUPOLE MAGNET DESIGN FOR THE ESS MEBT*

D. Fernández Cañoto[†], J. L. Muñoz, I. Rueda, G. Harper, S. Varnasseri, I. Bustinduy,
ESS Bilbao, Zamudio, Spain

Abstract

ESS Bilbao is responsible for the design and fabrication of the ESS MEBT as an In-Kind contribution. The MEBT includes a focusing lattice with 11 quadrupole magnets with different operational gradients, but fabricated from the same model to simplify manufacturing and save costs. The magnet is designed with a 20.5 mm aperture radius to generate focusing fields of up to 2.74 T and also includes two additional steering coil systems assembled around yoke return arms to produce vertical and horizontal dipole fields up to 20 G·m. The magnet model, which fabrication starts in 2017, is here introduced. Magnetic, thermoelectric and dimensional studies are performed and results compared to specifications. Suitable transfer functions for magnet operation and magnetic fields for a doublet system with a BCM magnetically shielded placed between the two magnets are presented.

INTRODUCTION

The Medium Energy Beam Transport (MEBT) line of the ESS linear accelerator (linac) is 3.8 m long and located between the radio frequency quadrupole (RFQ) and the drift tube linac (DTL) sections. The MEBT includes 11 magnets, 3 buncher cavities, 1 fast chopper, 1 beam dump, 2 beam scrappers and a wide variety of beam diagnostics [1, 2]. The magnets will be manufactured by the Danish company DANFYSIK [3].

The magnet is designed as an DC F-type normal quadrupole [4]. Vertical fields are produced from a steering coil system assembled around the left and right parts of the yoke return arms, and horizontal fields from a steering coil system assembled around the top and bottom parts of the yoke. Figure 1 shows a 3D drawing of the magnet assembly.

This paper starts with an introduction about the magnetic and mechanical models, including details about yoke and coil fabrication, magnet assembly, magnetic, thermoelectric and dimensional calculations. Results are compared to magnet specifications taken from reference [5]. Moreover, three transfer functions useful to describe magnetic strengths versus coil currents for single and combined field configurations are presented. Finally, magnetic fields for a doublet magnet system located at the end of MEBT line that includes a magnetically shielded combined beam current monitor (BCM) are analyzed.

MAGNET DESIGN

The MEBT section is rather small such that in order to install all of the equipment, geometric constrains have to be considered in every device. Hence, the magnet design is
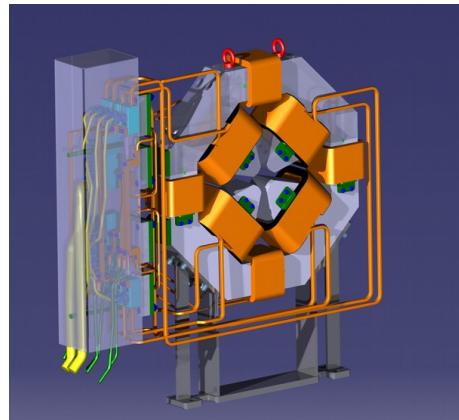
Figure 1: 3D magnet assembly.

not an exception and is biased to a high power low voltage model (low N, high I), longitudinally shorter than $L_{total} \leq$ 90 mm and transversally than $L_{trans} \leq 1200 \times 1200$ mm. Furthermore, a beam position monitor (BPM) [6] has to be installed between yokes and aligned with the magnet axial center constraining both the minimum inter-pole distance to $L_{p-p} \geq 14.5$ mm and the inter-coil separation to $L_{c-c} \geq$ 4.5 mm as shown in Fig. 2.
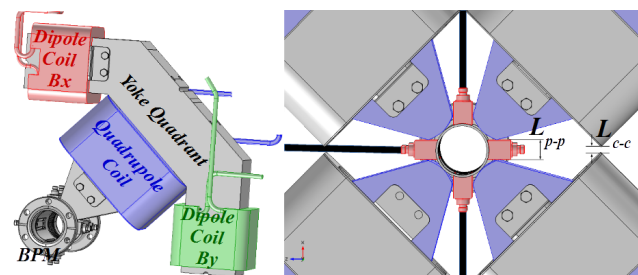
Figure 2: Quadrant assembly and embedded BPM.

Magnetic Model

The magnet has to generate at its center a quadrupole gradient of $g = \int g/L_{eff} = 34.25$ T/m and a dipole strength of $B_d = \int B_d/L_{eff} = 250$ G, where a magnetic length $L_{eff} = L_{yoke} + r \approx 80$ mm is considered for a yoke length of $L_{yoke} = 60$ mm. Ampère's Law is used to calculate the magneto-motive forces mmf being quadrupole force calculated as $mmf_q = gr^2/2\mu_0 = 5727$ A-turn, and the dipole force, for half a coil due to symmetry, as $mmf_d = B_d r/\mu_0 =$ 408 A-turn. Previous studies performed on coils geometry, power supply characteristics and reliability recommend a quadrupole coil with $I_q = 225$ A and $N_q = 27$ turns, and a dipole coil with $I_d = 8.25$ A and $N_d = 99$ turns. The optimum 2D yoke geometry is optimized by performing a

parametric study using an octant section comprised of a *pole tip* formed by a *hyperbolic section* from the points $(r, \theta) = (20.5[mm], 45[degrees])$ to $c = (x_c, y_c)$, a *shim section* to improve field quality and a *pole body* designed through *pole length*, *pole angle* and *line 1* parameters. A corner between *pole tip* and *pole body* becomes rounded at radius R. The octant is completed with the *return arm* part from *line 2* to *line 6*. Coil domains are represented by rectangular cross sections. 3D models can be designed by just rotating and extruding the octant. Volumetric coils are designed with racetrack shapes. Figure 3 shows 2D and 3D magnetic models, geometric parameters and optimization plots. Magnetic fields are calculated with COMSOL Multiphysics [7] and parameters evaluated at the good field region defined as GFR= $(x, y, z)|(x, y) \in \pi R_{GFR}^2, \forall z \in [-40, 40]$ mm, being $R_{GFR} = 15$ mm the reference radius. Figure 4 shows two magnetic 3D field distributions at the magnet middle plane $(x, y, 0)$ produced by quadrupole and dipole coil excitations.

Mechanical Model

The magnet assembly is comprised of an iron yoke divided in 4 quadrants, 4 quadrupole coils, 2 horizontal and 2 vertical dipole coils, 1 support feet, 1 thermo switch circuit for coil protection, and 1 services panel where electrical terminals and hydraulic manifold should be firmly installed. The iron yoke would be fabricated in a very low alloyed steel like ARMCO or similar with carbon content lower than 0.1 %, and coil conductors in Oxygen Free High Conductivity Copper (OFHC) 100% IACS. The quadrupole coil circuit is electrically connected in series and water-cooled in parallel. The dipole coil circuits are connected in series and refrigerated by natural air. A minimum number of brazed joints for coil tails, conductor leads and power terminals are considered. The magnet is assembled in two horizontal halves to facilitate assembly-disassembly and maintenance operations. Each of thermo-switch circuits is connected in series. 4 fiducial points required for magnet alignment are machined at the top of magnet.

Yoke: Each yoke quadrant would be assembled in two parts, a pole and return arm piece bolted together. Return arm lengths in two of the quadrants might be different to facilitate magnet assembly. Yoke pieces are cut from the same slab of steel. A CNC machine cuts, mills and drills steel blocks. Once the yoke is assembled final tolerances are achieved by a wire erosion machine.

Coils: *a) Quadrupole coil*: The conductor geometry is 5×5 mm quadrangular, with a $D_H = 3$ mm hollow diameter, $R_f = 0.7$ mm fillet radius and $L_q \approx 9.6$ m long. The conductor is insulated to prevent inter-turn voltage breakdown with E-glass fiber tape 0.13 mm thick treated with amino silane to reinforce chemical bonding with the Epoxy resin. The N_q turns are winded in 2 rows of 14 and 13 turns by means of a semi automatic machine that synchronizes winding and taping operations. The winding is over wrapped with extra layers of fiber to reinforce ground insulation. Coils are block
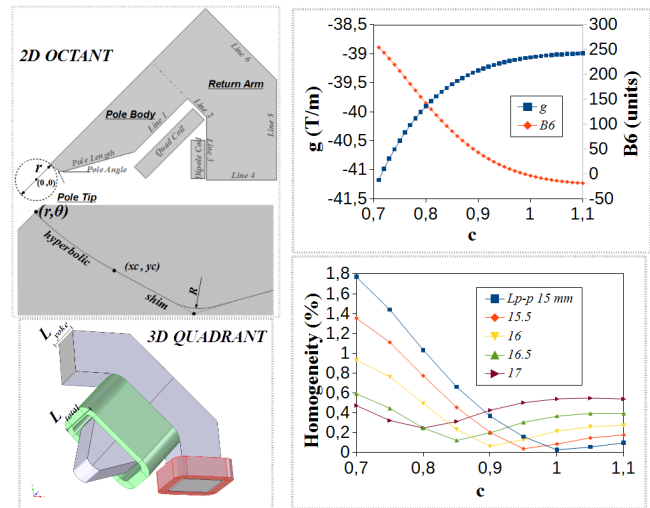
Figure 3: Magnetic models, geometric parameters and optimization plots.
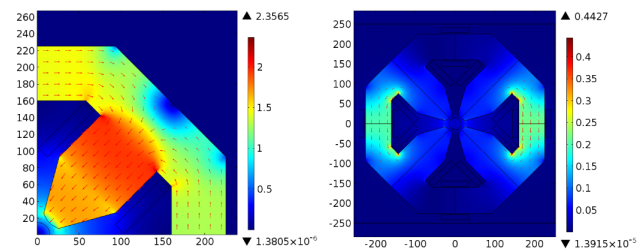
Figure 4: Quadrupole (left) and dipole (right) $|\vec{B}|$ field distributions given in Tesla at the $(x, y, 0)$ plane.

molded with a radiation resistant C Epoxy resin by means of a vacuum-pressure impregnation (VPI) technique and then cured in the oven.

b) Dipole coil: The conductor geometry is 1.25×4.5 mm solid rectangular, with $R_f = 1$ mm and $L_d \approx 17.5$ m long. The N_d turns are distributed in windings of 11 rows of 9 turns. Dipole coils would be winded and insulated with similar techniques as described for quadrupole coils.

Model Analysis

Magnetic, thermoelectric and dimensional analysis are carried out on the magnet model. Table 1 shows the comparison between analysis results and specifications.

TRANSFER FUNCTIONS

The first transfer function, $\mathcal{T}_q = \int g/I_q$, is calculated for the quadrupole strength, where simulations for $I_q \in [45, 225]$ A in $\Delta I_q = 15$ A steps being $I_d = 0$ A are used. The second one, $\langle \mathcal{T}_d \rangle$, is obtained for the dipole strength on a combined field configuration with quadrupole fields, where an average function of the $\mathcal{T}_d = \int B_d/I_d$ values taken from simulations at four dipole $I_d = 2, 4, 6, 8$ A currents versus I_q, is calculated. Both $\mathcal{T}_q$ and $\langle \mathcal{T}_d \rangle$ functions are fitted to fifth order polynomials and coefficients given in Table 2. The third function, $\mathcal{T}_{q_d}$, is calculated for the quadrupole strength

Table 1: Main Specifications vs. Analysis Results

Magnetic	Spec.	Quad.	Dip.
$\int g$ [T]	≥ 2.74	3.05	-
$\int B_d$ [G·m]	≥ 20	-	40
Harmonic$_{q,d_{N>3}}$[%]	$\leq [1, 10]$	0.3	1.1
Homogeneity$_{q,d}$ [%]	$\leq [1, 20]$	0.7	14
Fringe field [G]	≤ 100	95	-
Thermoelectric			
$I_{q,d}$[A]	$\leq [265, 20]$	225	8.25
Water velocity[m/s]	≤ 2	2	-
Pressure drop[bar]	≤ 2.42	2.8	-
Temperature drop[°C]	≤ 12	10	-
Mechanical			
L_{p-p}[mm]	≥ 14.5	15.9	-
L_{c-c}[mm]	≥ 4.0	15.5	-
L_{total}[mm]	≤ 90	89.1	-
L_{trans}[mm]	$\leq 1200 \times 1200$	732×569	-

also combined with dipole fields, where the $\mathcal{T}_{q_d} = \int g / I_q$ values versus I_d are mapped on a $I_d \times I_q$ grid by means of spline interpolations. Transfer function plots are given in Fig. 5.

Table 2: Polynomial Fit Coefficients for $\langle \mathcal{T}_d \rangle$ and $\mathcal{T}_q$

	a5	a4	a3	a2	a1	a0
$\langle \mathcal{T}_d \rangle$	1.6E−14	−9.7E−12	2.1E−9	−2.1E−7	9.7E−6	3.4E−4
$\mathcal{T}_q$	9.7E−14	−6.5E−11	1.6E−8	−1.7E−6	8.7E−5	1.4E−2
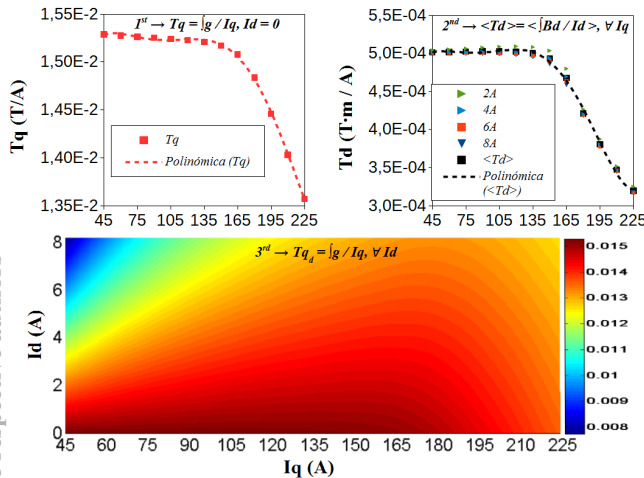
Figure 5: Transfer functions versus coil currents.

MAGNETIC FIELDS FOR A DOUBLET WITH A SHIELDED BCM

Magnetic fields are investigated for a doublet magnet system located at the end of MEBT line that has in the middle a BCM magnetically shielded. The BCM consists of an AC current transformer (ACCT) toroid and a fast current transformer FCT system to measure beam current and

charge [8]. The complete BCM is externally shielded as depicted in Fig. 6, where a cylindrical framework 5 mm thick made of soft iron, two 1 mm thick Mu-metal extra layers for ACCT and one for FCT are added. The two quadrupole coil currents are set to its maximum at $I_q = 225$ A and magnetic fields calculated with and without shielding. Figure 6 shows quadrupole gradients versus z and the $|\vec{B}|$ field distribution at BCM magnetic core surfaces. The total integrated quadrupole field downstream the doublet with a shielded BCM can be decreased up to a $\sim 4\%$.
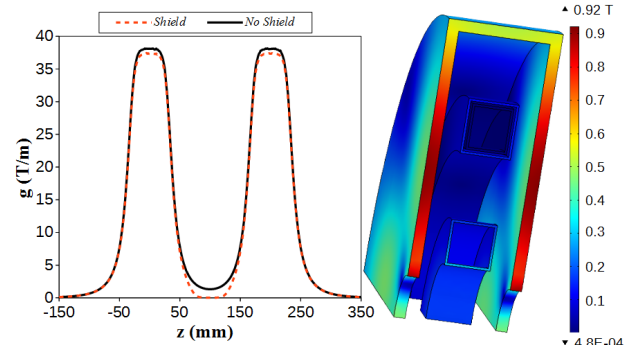
Figure 6: Comparison of g vs z with and without shielding (left), and BCM core surface $\vec{B}$ field.

CONCLUSIONS

The MEBT magnet design has been presented and the analysis has demonstrated its feasibility for manufacturing. Transfer functions for single and combined magnetic fields operated at any current can facilitate magnet operation. The integrated quadrupole strength calculated for a doublet system located at the MEBT end with a BCM magnetically shielded can be decreased up to a maximum of $\sim 4\%$.

REFERENCES

[1] S. Peggs *et al.*, "ESS Technical Design Report", ESS Report, April (2013).

[2] I. Bustinduy *et al.*, "Medium energy beam transport design update for ESS", in *Proc. HB'12*, Beijing, China, Sep. 2012, pp. 128–132.

[3] Danfysik A/S, Gregersensvej 8, DK-2630 Taastrup, Denmark.

[4] J. Tanabe, "Iron dominated electromagnets - design, fabrication, assembly and measurements ", SLAC, Stanford, CA, USA, Rep. SLAC-R-754, Jun. 2005.

[5] D. Fernández Cañoto, J.L. Muñoz, and I. Bustinduy, "Magnetic design and specifications of a quadrupole magnet for the MEBT", ESS Bilbao, Spain, Rep. ESSB-2016-20, Jun. 2016.

[6] S. Varnasseri *et al.*, "Design of a BPM stripline for the ESS MEBT", in *Proc. IBIC'16*, Barcelona, Spain, Sep. 2016, pp. 620–622.

[7] COMSOL Multiphysics, www.comsol.com

[8] H. Hassanzadegan *et al.*, "Beam current monitor system of the European Spallation Source", in *Proc. LINAC'14*, Geneva, Switzerland, Aug.-Sep. 2014, pp. 526–528.